

Effects of Lithium Content on the Structure and Electrochemical Performance of Spherical Lithium-rich Cathode Materials

LIU Jin-long¹, YANG Jun¹, GUO Shao-shuai¹, WANG Yong-gang¹,
WANG Cong-xiao¹, LIU Hai-mei², XU Qun-jie², XIA Yong-yao¹

(1. Department of Chemistry, Shanghai Key Laboratory of Molecular Catalysis and Innovative Materials, Institute of New Energy, Collaborative Innovation Center of Chemistry for Energy Materials, Fudan University, Shanghai 200433, China; 2. Shanghai University of Electric Power, Shanghai 200215, China)

ABSTRACT: Lithium-rich cathode materials have become one of the most promising cathode materials for high-energy-density lithium-ion batteries. However, the electrochemical properties of lithium-rich cathode materials are highly sensitive to the local structure in the bulk and at the surface, which is closely associated with the synthesis process. In the present work, we provided new insights into the structural properties and corresponding electrochemical performance of $\text{Li}_{1.2x}\text{Mn}_{0.54}\text{Ni}_{0.13}\text{Co}_{0.13}\text{O}_2$ materials as a function of x (Li content) from a synthesis point of view. The spinel and Li_2CO_3 species in the bulk and at the surface arising from the varying amounts of lithium ions would result in the local compositional change within the as-prepared particles and provoke a change in the voltage-capacity profile as determined by electrochemical analysis, XRD, Raman, and XPS observations. Our results revealed that the as-prepared sample with 5% excess of Li in molar ratio utilized for the material synthesis showed better electrochemical performance in terms of discharge capacity (~ 270 mAh/g) and voltage in comparison to other as-prepared samples with different Li contents.

KEY WORDS: batteries; lithium-rich cathode materials; layered; spherical; local structure

中图分类号: TQ131.1; TM912 文献标识码: A 文章编号: 1001-3660(2015)01-0015-09

Li 含量对球形富锂正极材料结构和电化学性能的影响

刘金龙¹, 杨军¹, 郭少帅¹, 王永刚¹, 王丛笑¹, 刘海梅², 徐群杰², 夏永姚¹

(1. 复旦大学, 能源材料化学协同创新中心, 新能源研究院, 上海市分子催化与功能材料重点实验室, 化学系, 上海 200433; 2. 上海电力学院, 上海 200215)

摘要: 富锂正极材料已经成为高能量密度锂离子电池最具有前景的正极材料之一。然而, 富锂正极材料电化学性能对其本体和表面的局域结构很敏感, 而这些结构跟材料的合成过程密切相关。在目前的工作中, 从合成的角度提出了新的思路, Li 含量 x 将影响着富锂 $\text{Li}_{1.2x}\text{Mn}_{0.54}\text{Ni}_{0.13}\text{Co}_{0.13}\text{O}_2$ 材料的结构特性和

Received : 2015-01-01; **Revised:** 2015-01-08

收稿日期: 2015-01-01; **修订日期:** 2015-01-08

Fund: Supported by the State Key Basic Research Program of PRC (2011CB935903), the National Natural Science Foundation of China (21333002 and 20925312), and Shanghai Science & Technology Committee (13JC1407900, 10JC1401500 and 08DZ2270500).

基金项目: 科技部纳米重大专项(2011CB935903); 国家自然科学基金项目(21333002 and 20925312); 上海市科委基础重点项目(13JC1407900, 10JC1401500, 08DZ2270500)

Corresponding author: XIA Yong-yao (1965—), Male, from Zhejiang, Ph. D., Professor, Research focus: electrochemistry, advanced technology and materials for energy storage and conversion devices.

通讯作者: 夏永姚(1965—), 男, 浙江人, 博士, 教授, 主要从事电化学、化学储能技术及其材料方面的研究。

电化学性能。基于电化学, XRD, Raman, XPS 技术的分析结果, 改变 Li 含量将在材料的本体和表面产生尖晶石相和 Li_2CO_3 物种, 会造成所合成的材料局部组分发生变化, 进而影响其电压容量曲线。实验结果表明, 在正极材料合成的过程中, 相比于其他含量, Li 含量过量 5% (摩尔分数) 所合成的样品表现出更好的电化学性能, 放电容量高达 270 mAh/g。

关键词: 电池; 富锂正极材料; 层状; 球形; 局域结构

1 Introduction

Lithium-rich cathode materials, represented in solid solution notation as $\text{Li}[\text{Ni}_x\text{Li}_{(1-2x)/3}\text{Mn}_{(2-x)/3}]\text{O}_2$ ($0 < x < 0.5$) or by the general formula $x\text{Li}_2\text{MnO}_3 \cdot (1-x)\text{LiMO}_2$ ($\text{M} = \text{Mn}, \text{Co}, \text{Ni}, \text{etc.}$), have been recognized as one of the most promising cathode materials for high-energy-density lithium-ion batteries (LIBs) owing to their high reversible capacities of $\sim 250 \text{ mAh/g}$ [1–7]. Intensive investigations to interpret the fundamental lithiation-delithiation mechanism in lithium-rich cathode materials have revealed that the abnormally high capacity originates either from the removal of oxygen from the lattice accompanied by lithium extraction involving cationic ($\text{M}^{n+}/\text{M}^{n+1}$) and anionic ($\text{O}^{2-}/\text{O}_2^{2-}$) reversible redox processes [5–10], or from the surface reaction through electrode/electrolyte reduction with the formation of Li_2CO_3 species, and/or Li^+/H^+ exchange in the bulk particles [11–12], though there is an ongoing debate in prior studies on the detailed mechanisms and their complex crystal structure [5–6, 13]. However, lithium-rich cathode materials suffer from a large irreversible capacity loss ascribable to lithium consumption and electrolyte oxidation in the first cycle [5, 14–15], poor rate capability arising from the slow kinetics of oxygen diffusion or electron/lithium-ion transport [15–18], and the severe voltage degradation upon electrochemical cycling associated with the migration of transition-metal cations [19–21], which have gapped them from the widespread practical applications.

To circumvent these challenges, new strategies have been developed to synthesize and stabilize electrode structure of advanced lithium-rich transition-metal oxides [21–35]. Recently, Sun and co-workers developed a crystal habit-tuned nanoplate material of $\text{Li}[\text{Li}_{0.17}\text{Ni}_{0.25}\text{Mn}_{0.58}]\text{O}_2$ with a high rate capability, in which the proportion of (010) nanoplates was significantly increased [22]. Thackeray et

al. proposed a versatile approach to fabricate $x\text{Li}_2\text{MnO}_3 \cdot (1-x)\text{LiMO}_2$ composites with insignificant voltage shape change using a Li_2MnO_3 template into which the desired M cations can be introduced via an acid-treatment process, followed by an annealing step [26]. Very recently, our work demonstrated that layered lithium-rich transition-metal oxides with various degrees of stacking faults were successfully prepared via a molten-salt method using KCl, Li_2CO_3 , and LiNO_3 fluxes, which showed substantially improved electrochemical properties when the amount of stacking faults within the crystal structure was increased [28]. Furthermore, surface modification with electrochemically inactive oxides (e.g. Al_2O_3 , AlPO_4 , and ZrO_2 etc.) as well as electrochemically active compounds (e.g. MnO_x , LiNiPO_4 , and etc.) has been employed with some promising results in terms of rate capability and initial coulombic efficiency [29–35]. Such improvements are attributed to the interfacial protection layer between the cathode and the electrolyte and electron/ion-conducting media that facilitates the charge transfer at the surface of the particles [36–37].

As a matter of fact, prior studies mentioned above have demonstrated that the electrochemical performance of lithium-rich cathode materials are strongly influenced by the local structure in the bulk and at the surface of the particles, which is highly associated with the synthesis process. Furthermore, many research groups have reported that the lithium-rich cathode materials prepared via a co-precipitation method show various electrochemical properties; however, the differences are not clearly clarified at present. To shed some light on this issue and to get a better understanding of lithium-rich cathode materials, we systemically investigated the local composition in the bulk and at the surface and the corresponding electrochemical properties of $\text{Li}_{1.2x}\text{Mn}_{0.54}\text{Ni}_{0.13}\text{Co}_{0.13}\text{O}_2$ materials as a function of x utilized for the material synthesis through careful analysis of XRD, Raman, and

XPS observations in the present work.

2 Experimental

2.1 Synthesis of materials

The $\text{Li}_{1.2x}\text{Mn}_{0.54}\text{Ni}_{0.13}\text{Co}_{0.13}\text{O}_2$ ($x=0.95, 1.00, 1.05, 1.10$, and 1.15) materials were synthesized by solid-state reaction of varying amounts of Li_2CO_3 and the spherical Ni-Co-Mn precursor oxide (Ni : Co : Mn molar ratio of $0.13 : 0.13 : 0.54$). After well mixing, the mixture was placed in an alumina crucible, heated to $900\text{ }^\circ\text{C}$ in air in a box furnace at a heating rate of $5\text{ }^\circ\text{C}/\text{min}$ for 10 h, and then quenched to room temperature in air.

The spherical Ni-Co-Mn precursor oxide was prepared by a co-precipitation method. A 2 M aqueous solution of NiSO_4 , CoSO_4 and MnSO_4 (Ni : Co : Mn = $0.13 : 0.13 : 0.54$ in the molar ratio) was mixed with a 2 M aqueous solution of NaOH with desired amount of 0.2 M NH_4OH as a chelating agent in a continuously stirred tank reactor (CSTR) at a constant pH of ~ 11 under a flow of nitrogen at $60\text{ }^\circ\text{C}$. Finally, the product was washed with distilled water several times, filtered, dried in an air oven at $80\text{ }^\circ\text{C}$ for 24 h, and then the powder was sintered at $500\text{ }^\circ\text{C}$ for 5 h.

2.2 Characterization of materials

Powder X-ray diffraction (XRD) measurements were performed on a Rigaku D/MAX-IIA X-ray diffractometer equipped with a Cu-K α radiation source (Bruker, Germany) in the 2θ range of $10^\circ \sim 80^\circ$ at 2θ step-scan intervals of 0.02° with a step time of 0.5 s. The particle morphologies of the samples were observed with a Hitachi S-4800 scanning electron microscopy (SEM) operated at 20 kV. Raman measurements were performed in a back-scattered configuration using a micro-Raman spectrometer LabRam HR 800 equipped with an Ar⁺ laser ($\lambda = 632.8\text{ nm}$) from Jobin-Yvon Horiba Inc. at room temperature. X-ray photoelectron spectroscopy (XPS) measurements were performed on a PHI 5000C ESCA system with Mg K α source operated at 14.0 kV and 25 mA. The energies of the spectra were calibrated

by the binding energy of C 1s at 284.6 eV as a reference.

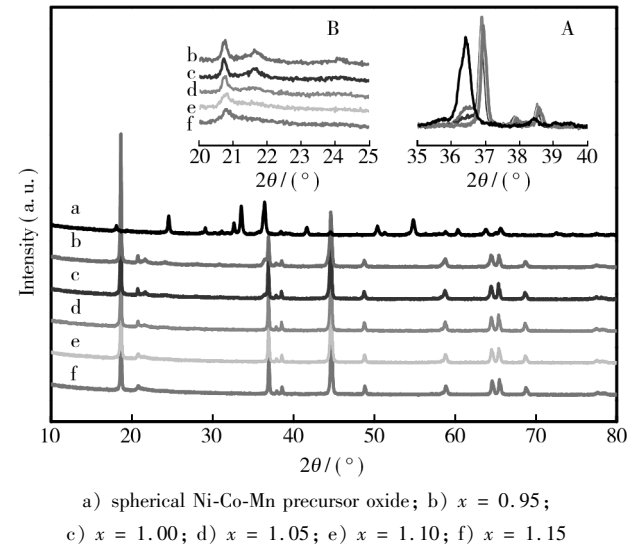
2.3 Electrochemical tests

The electrochemical measurements were performed in CR2016-type coin cells. For the preparation of the $\text{Li}_{1.2x}\text{Mn}_{0.54}\text{Ni}_{0.13}\text{Co}_{0.13}\text{O}_2$ electrodes, 80 wt% of active material, 10 wt% carbon black conductive materials, and 10 wt% polyvinylidene difluoride (PVDF) binder were mixed in N-methyl-2-pyrrolidone (NMP) solvent. Then, the slurry was cast onto an aluminum-foil current collector. After coating, the electrodes were dried at $80\text{ }^\circ\text{C}$ for 10 h to remove the solvent before being pressed. The electrode film was punched in the form of disks, typically with a diameter of 12 mm, and then dried at $80\text{ }^\circ\text{C}$ for 12 h under vacuum. The typical mass loading of the active material of the working electrodes was approximately 5 mg. The cells were assembled with the cathode as prepared, lithium metal as anode, and Celgard 2300 film as separator in a glove-box filled with pure argon. The electrolyte solution was 1 M LiPF_6 dissolved in ethylene carbonate (EC)/dimethyl carbonate (DMC)/ethyl methyl carbonate (EMC) ($1 : 1 : 1$ by volume). Galvanostatic charge/discharge experiments were performed between 2.0 and 4.8 V at room temperature ($30\text{ }^\circ\text{C}$) with a LAND CT2001A Battery Cycler (Wuhan, China). Lithium intercalation into the working electrode was referred to as discharge, and the de-intercalation as charge. The cell capacity was calculated based on the weight of the active material.

3 Results and discussion

The crystal structures of the as-prepared $\text{Li}_{1.2x}\text{Mn}_{0.54}\text{Ni}_{0.13}\text{Co}_{0.13}\text{O}_2$ ($x=0.95, 1.00, 1.05, 1.10$, and 1.15) series were confirmed by power X-ray diffraction (XRD) as shown in Fig. 1. For comparison, the XRD pattern of spherical Ni-Co-Mn precursor oxide was measured. As presented in Fig. 1, the sharp Bragg peaks could be indexed in the hexagonal R-3m unit cell, except for the additional broadened superstructure lines in the 2θ range of $20^\circ \sim 25^\circ$. These superstructure peaks were the features of structurally integrated monoclinic (C2/m) Li_2MnO_3 -like component ascribable to lithium-cation or-

dering in the transition-metal layers. The broadening of the superlattice peaks resulted from stacking faults in the ordered cationic planes occurred along the *c* monoclinic axis as demonstrated in prior studies^[5,28]. All of these characteristic peaks were present in the XRD patterns of the as-prepared $\text{Li}_{1.2x}\text{Mn}_{0.54}\text{Ni}_{0.13}\text{Co}_{0.13}\text{O}_2$ series, which were consistent with the previous reported results^[5]. However, detailed peak changes could be found in the selective patterns in the ranges of $20^\circ \sim 25^\circ$ and $35^\circ \sim 40^\circ$. As depicted in Fig.1 inset A, the Bragg peaks belonging to spherical Ni-Co-Mn precursor oxide in the XRD patterns of as-prepared $\text{Li}_{1.2x}\text{Mn}_{0.54}\text{Ni}_{0.13}\text{Co}_{0.13}\text{O}_2$ materials progressively disappeared when the Li content (*x*) increased, suggesting an evaporative lithium loss during the calcination and the complete reaction between the raw Ni-Co-Mn precursor oxide and excess of Li ions. Moreover, it should be noted that the disappearance of the (110) superlattice peaks in the 2θ range of $20^\circ \sim 25^\circ$ was observed with an increase in the amount of Li ions during the synthesis process as shown in Fig.1 inset



The inset A marks the peaks related to the Ni-Co-Mn precursor oxide. The inset B highlights the superlattice peaks in the 2θ range of $20^\circ \sim 25^\circ$

Fig.1 XRD patterns of the spherical Ni-Co-Mn precursor oxide and the final as-obtained $\text{Li}_{1.2x}\text{Mn}_{0.54}\text{Ni}_{0.13}\text{Co}_{0.13}\text{O}_2$ powders prepared at 900°C for 10 h with varying amounts of Li ions via a co-precipitation method

图1 球形 Ni-Co-Mn 氧化物前驱体及其与不同含量 Li 盐煅烧后合成的 $\text{Li}_{1.2x}\text{Mn}_{0.54}\text{Ni}_{0.13}\text{Co}_{0.13}\text{O}_2$ 样品的 XRD 谱图(插图 A 表示 Ni-Co-Mn 氧化物前驱体相关衍射峰,插图 B 表示 $20^\circ \sim 25^\circ$ 范围的超晶格衍射峰。): a) 球形氧化物前驱体; b) $x = 0.95$; c) $x = 1.00$; d) $x = 1.05$; e) $x = 1.10$; f) $x = 1.15$

B. Two weak peaks were clearly observed in the XRD patterns of as-prepared $\text{Li}_{1.2x}\text{Mn}_{0.54}\text{Ni}_{0.13}\text{Co}_{0.13}\text{O}_2$ ($x = 0.95$, and 1.00) materials; however, only a single superstructure peak at 20.9° was detected when x increased to 1.15 , implying an increase in the amount of stacking faults within the as-prepared particles, which is not well understood at present.

Fig.2 shows the typical morphologies of the precursor oxide and the final lithiated oxides prepared at 900°C for 10 h with varying amounts of Li ions. As evident in the SEM images, the diameter of the spherical precursor oxide particles was in the range of about $5 \sim 10\ \mu\text{m}$, which consisted of primary irregular nanoparticles with an average diameter close to $200\ \text{nm}$. After the lithiation at high temperature, each as-obtained sample was still

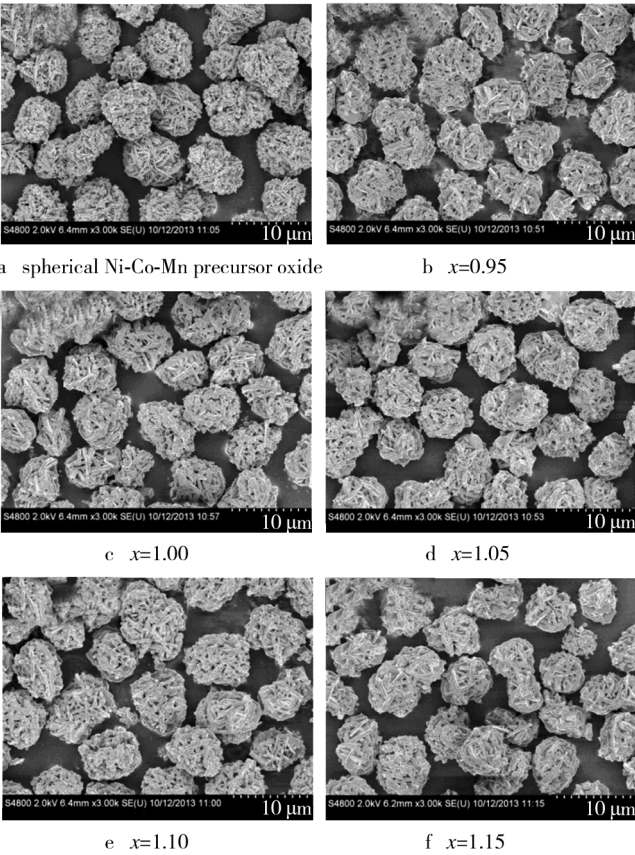


Fig.2 SEM images of the spherical Ni-Co-Mn precursor oxide and the final as-obtained $\text{Li}_{1.2x}\text{Mn}_{0.54}\text{Ni}_{0.13}\text{Co}_{0.13}\text{O}_2$ materials prepared at 900°C for 10 h with varying amounts of Li ions via a co-precipitation method

图2 球形 Ni-Co-Mn 氧化物前驱体及其与不同含量 Li 盐煅烧后合成的 $\text{Li}_{1.2x}\text{Mn}_{0.54}\text{Ni}_{0.13}\text{Co}_{0.13}\text{O}_2$ 样品的 SEM 照片: a) 球形氧化物前驱体; b) $x = 0.95$; c) $x = 1.00$; d) $x = 1.05$; e) $x = 1.10$; f) $x = 1.15$

composed of spherical particles with diameters in the range of 5 ~ 10 μm. Besides, the lithiation at high temperature resulted in larger primary particle sizes (~500 nm) compared to the precursor oxide. However, no obvious morphology changes were detected for the final lithiated oxides prepared at 900 °C for 10 h with an increase in Li content, as evidenced in Fig. 2.

In order to determine the local composition in the bulk and at the surface, and to further track the compositional change within the particles of the as-prepared materials, Raman spectroscopy and X-ray photoelectron spectroscopy (XPS) analyses were carried out for the precursor oxide and the final lithiated oxides with varying amounts of Li ions. Raman spectroscopy has been recognized as one of the most sensitive tools to detect unique molecular and structural information at the atomic scale by determination of frequencies of normal vibrations^[38]. Fig. 3 shows Raman spectra of the spherical precursor oxide and the final lithiated oxides obtained at 900 °C for 10 h with different Li contents. As shown in Fig. 3, three major peaks in the Raman spectrum were observed at ca. 604, 487, and 430 cm⁻¹ for each as-prepared Li_{1.2x}Mn_{0.54}Ni_{0.13}Co_{0.13}O₂ cathode material. This result agreed well with those reported in previous studies^[19] and was consistent with the theoretical prediction given for a hexagonal (R-3m) and a monoclinic (C2/m)

crystal^[38], respectively. Generally, there were two Raman-active vibrational modes in the ideal layered lithium transition metal oxide with R-3m symmetry: A_{1g} with the symmetrical stretching of M-O and E_g with the symmetrical deformation, which corresponded to two sharp Raman peaks near 604 cm⁻¹ and 487 cm⁻¹, respectively. An additional small Raman band at 430 cm⁻¹ originated from the Li₂MnO₃-like structure due to the reduced local symmetry of C2/m rather than R-3m, indicating the presence of Li₂MnO₃ short-range superlattice ordering. Notably, the Raman peaks assigned to the Ni-Co-Mn precursor oxide in the Raman spectra of the as-prepared Li_{1.2x}Mn_{0.54}Ni_{0.13}Co_{0.13}O₂ particles disappeared with the increase in Li content utilized for material synthesis, which implied the complete reaction between the raw Ni-Co-Mn precursor oxide and Li-salt, in perfect agreement with the XRD observation. However, with further increase of the Li content, a new weak peak started evolving between 500 and 600 cm⁻¹, which was attributed to the formation of spinel phase^[19]. However, it was clear that no significant diffraction peaks of the spinel phase could be detected in the XRD patterns as illustrated in Fig. 1, suggesting the formation of a small amount of spinel nanodomains which were smaller than the X-ray coherence length. Therefore, this result provided by Raman spectroscopy demonstrated that excess of Li ions during the synthesis process could generate a small amount of spinel phase impurity in the local structure of the as-prepared lithium-rich transition metal oxides, which would give rise to the obvious changes in electrochemical performance as discussed in the later section.

Fig. 4 depicts the XPS spectra of O 1s and C 1s regions observed for the spherical Ni-Co-Mn precursor oxide and lithium-rich transition metal oxides samples prepared at 900 °C to examine the local composition at the surface, respectively. As seen in Fig. 4, two peaks characteristic of O²⁻ anions in the O 1s spectrum were observed with the increase in Li content: the peak at 529.5 eV belonged to the O²⁻ ions in the transition-metal oxide crystalline network and the peak at 531 eV corresponded to the O²⁻ ions ascribable to weakly adsorbed surface species CO₃²⁻^[10,12]. The observation of the carbonate species indicated the existence of Li₂CO₃ at the surface

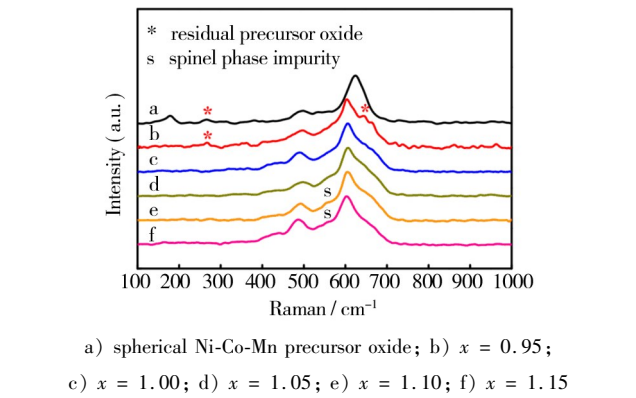
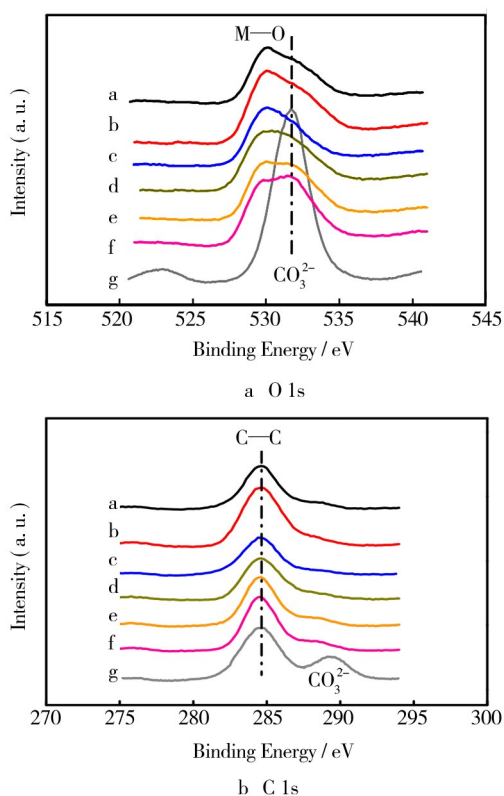


图 3 球形 Ni-Co-Mn 氧化物前驱体及其与不同含量 Li 盐煅烧后合成的 Li_{1.2x}Mn_{0.54}Ni_{0.13}Co_{0.13}O₂ 样品的 Raman 图谱 (* 表示残留的氧化物前驱体, s 表示尖晶石杂相): a) 球形氧化物前驱体; b) x = 0.95; c) x = 1.00; d) x = 1.05; e) x = 1.10; f) x = 1.15



a) spherical Ni-Co-Mn precursor oxide; b) $x = 0.95$; c) $x = 1.00$; d) $x = 1.05$; e) $x = 1.10$; f) $x = 1.15$; g) Li_2CO_3

Fig. 4 XPS spectra of O 1s and C 1s regions observed for the spherical Ni-Co-Mn precursor oxide, lithium-rich transition metal oxides $\text{Li}_{1.2x}\text{Mn}_{0.54}\text{Ni}_{0.13}\text{Co}_{0.13}\text{O}_2$, and Li_2CO_3 powder

图 4 球形 Ni-Co-Mn 氧化物前驱体及其与不同含量 Li 盐煅烧后合成的 $\text{Li}_{1.2x}\text{Mn}_{0.54}\text{Ni}_{0.13}\text{Co}_{0.13}\text{O}_2$ 以及 Li_2CO_3 的 O1s 和 C1s 图谱: a) 球形氧化物前驱体; b) $x = 0.95$; c) $x = 1.00$; d) $x = 1.05$; e) $x = 1.10$; f) $x = 1.15$; g) Li_2CO_3

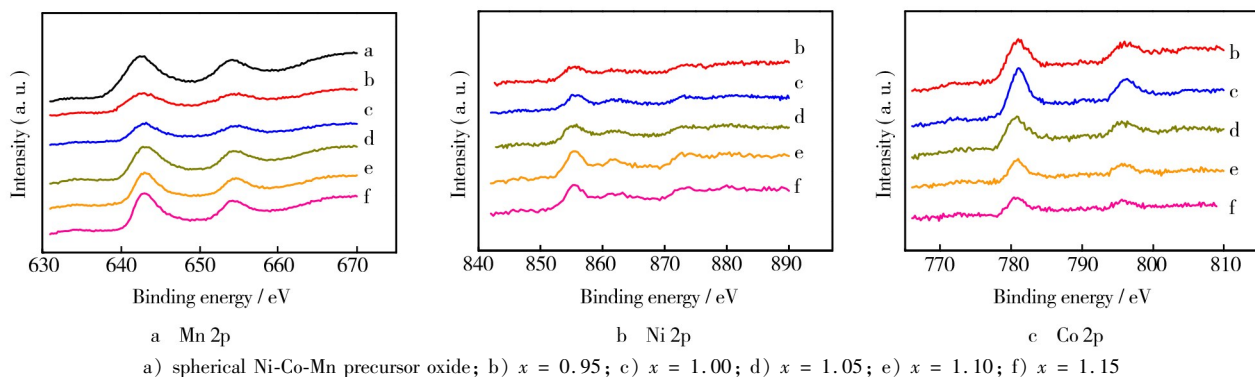


Fig. 5 XPS spectra of Mn 2p, Ni 2p, and Co 2p regions observed for the precursor oxide and the final as-obtained $\text{Li}_{1.2x}\text{Mn}_{0.54}\text{Ni}_{0.13}\text{Co}_{0.13}\text{O}_2$ materials prepared at 900 °C for 10 h with varying amounts of Li ions via a co-precipitation method

图 5 球形 Ni-Co-Mn 氧化物前驱体及其与不同含量 Li 盐煅烧后合成的 $\text{Li}_{1.2x}\text{Mn}_{0.54}\text{Ni}_{0.13}\text{Co}_{0.13}\text{O}_2$ 样品 Mn 2p, Ni 2p 和 Co 2p 图谱: a) 球形氧化物前驱体; b) $x = 0.95$; c) $x = 1.00$; d) $x = 1.05$; e) $x = 1.10$; f) $x = 1.15$

of the final lithiated oxide particles because the over stoichiometric Li ions were used for the synthesis of $\text{Li}_{1.2x}\text{Mn}_{0.54}\text{Ni}_{0.13}\text{Co}_{0.13}\text{O}_2$ ($x = 1.10$, and 1.15). Moreover, the intensity of the shoulder peak at 531 eV assigned to Li_2CO_3 species increased with the increasing Li content during the synthesis process, implying an increase in the amount of residual excess of Li ions on the surface of the final lithiated oxides. Turning to the C 1s spectrum as presented in Fig. 4, the main sharp C—C peak at the 284.6 eV was attributed to the "adventitious carbon" as a reference and another weak peak at 289.4 eV was associated with carbonate species at the surface of the final lithiated oxides^[10,27]. With the increase in Li content utilized for material synthesis, the weak peak originated from Li_2CO_3 species started evolving at 289.4 eV, further confirming that the partial excess of Li ions resulted in the formation of a small amount of Li_2CO_3 at the surface of the final lithiated oxides in perfect agreement with the previous O 1s XPS spectrum observations.

Fig. 5 shows the XPS spectra of Mn 2p, Ni 2p, and Co 2p regions observed for the precursor oxide and final lithium-rich transition metal oxides prepared at 900 °C to examine the oxidation state of transition metals at the surface, respectively. As depicted in Fig. 5, two peaks were clearly visible, which were associated with the manganese $2p_{3/2}$ at 642 eV and $2p_{1/2}$ at 654 eV and agreed well with the literatures data on MnO_2 ^[12]. However, no significant difference was detected by XPS for the as-prepared materials with varying amounts of Li salt in this experiment. From the Ni 2p and Co 2p XPS spec-

tra, the observations were consistent with the results in the Mn 2p spectra as shown in Fig. 5, indicating no significant difference in the oxidation state of transition metals at the surface of the final lithiated oxides.

Therefore, based on the Raman spectroscopy and X-ray photoelectron spectroscopy (XPS) analyses, the findings are summarized as follows. With the increase in Li content, a small amount of Li_2CO_3 was found at the surface of the final lithiated oxides, which was consistent with the fact that excessive Li_2CO_3 in molar ratio was utilized for the material synthesis. The excessive Li ions during the synthesis process could compensate for any evaporative lithium loss during the calcinations, resulting in the formation of spinel phase in the local structure, and generating a small amount of Li_2CO_3 at the surface of the lithium-rich transition metal oxide, which further led to slight deviation of the as-prepared lithium-rich transition metal oxides from the local composition and structure of ideal layered $\text{Li}_{1.2}\text{Mn}_{0.54}\text{Ni}_{0.13}\text{Co}_{0.13}\text{O}_2$ cathode material.

Fig. 6 presents the typical initial charge-discharge curves of the as-prepared $\text{Li}_{1.2x}\text{Mn}_{0.54}\text{Ni}_{0.13}\text{Co}_{0.13}\text{O}_2$ electrodes in the potential range of 2.0 ~ 4.8 V at a current density of 20 mA/g at room temperature. When initially charged to 4.8 V, the electrochemical reaction of lithium with the $\text{Li}_{1.2x}\text{Mn}_{0.54}\text{Ni}_{0.13}\text{Co}_{0.13}\text{O}_2$ electrodes occurred in two distinct steps, as follows: the first step measured at voltage < 4.4 V vs. Li/Li^+ corresponded to lithium extraction from the LiMO_2 component with the concomitant oxidation of Ni^{2+} to Ni^{4+} and Co^{3+} to Co^{4+} ; and the second step corresponded to the removal of lithium from the crystal structure accompanied by oxygen evolution when charged above 4.4 V vs. Li/Li^+ according to the prior studies [5]. Notably, all the samples showed similar voltage profiles during the initial charge, however, significantly different discharged curves were clearly observed as shown in Fig. 6. The increase in Li content (x) utilized for the material synthesis provoked a change in the voltage-capacity profile: the marked voltage variation was observed during the discharge and a new voltage plateau started evolving at ca. 2.7 V when $x \geq 1.10$. This was resulted from the emergence of a small amount of spinel-phase impurity and Li_2CO_3 species at the sur-

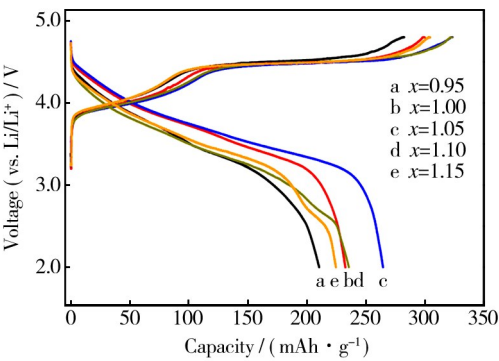


Fig. 6 Typical initial charge-discharge curves examined at a current density of 20 mA/g for the $\text{Li}_{1.2x}\text{Mn}_{0.54}\text{Ni}_{0.13}\text{Co}_{0.13}\text{O}_2$ electrodes prepared at 900 °C for 10 h with varying amounts of Li ions via a co-precipitation method

图 6 不同 Li 含量的 $\text{Li}_{1.2x}\text{Mn}_{0.54}\text{Ni}_{0.13}\text{Co}_{0.13}\text{O}_2$ 电极首圈充放电曲线(电流密度为 20 mA/g)

face of the final lithiated oxides as demonstrated by the previous Raman and XPS observations because excessive Li_2CO_3 in molar ratio was used during the synthesis process. Finally, the as-prepared sample with 5% excess of Li ions in molar ratio utilized for the material synthesis showed the largest reversible discharge capacity of ~270 mAh/g with the highest discharge voltage in comparison to other as-prepared samples with varying amounts of Li ions, indicating that Li content had a direct influence on the voltage profiles of lithium-rich transition metal oxides cathode materials.

Fig. 7 illustrates the cyclic performance of the $\text{Li}_{1.2x}\text{Mn}_{0.54}\text{Ni}_{0.13}\text{Co}_{0.13}\text{O}_2$ electrodes when cycled between 2.0 and 4.8 V at room temperature (30 °C). Upon cycling, the cells were charged-discharged at a current density of 20 mA/g in the initial 6 cycles, and then cycled at a current density of 200 mA/g during the subsequent cycles. The $\text{Li}_{1.2x}\text{Mn}_{0.54}\text{Ni}_{0.13}\text{Co}_{0.13}\text{O}_2$ ($x = 1.05$) electrode exhibited a gradual capacity fading upon cycling with an average capacity loss of ~0.2 mAh/g per cycle during cycling, that is, the discharge capacity of the $\text{Li}_{1.2x}\text{Mn}_{0.54}\text{Ni}_{0.13}\text{Co}_{0.13}\text{O}_2$ ($x = 1.05$) electrode maintained 88% of its initial capacity, suggesting good cyclic performance. It was noted that the $\text{Li}_{1.2x}\text{Mn}_{0.54}\text{Ni}_{0.13}\text{Co}_{0.13}\text{O}_2$ ($x = 1.10$) electrode with a small amount of spinel phase showed a good rate capability and cycling life. However, the reversible discharge capacities of other $\text{Li}_{1.2x}\text{Mn}_{0.54}$ -

$\text{Ni}_{0.13}\text{Co}_{0.13}\text{O}_2$ ($x = 0.95, 1.00, \text{ and } 1.10$) electrodes showed an increase in the initial 6 cycles, at least to some extent, and finally a slight capacity fading in the successive cycling. This indicated the gradual electrochemically activation of the final lithiated oxide electrodes, which was most likely ascribed to the impurities in the bulk and at the surface due to the varying amounts of Li ions utilized for the material synthesis, thereby deviating the as-prepared lithium-rich transition metal oxides from the ideal composition of layered $\text{Li}_{1.2}\text{Mn}_{0.54}\text{Ni}_{0.13}\text{Co}_{0.13}\text{O}_2$, providing significantly varying electrode/electrolyte interface, and showing different electrochemical properties of the as-prepared materials. As a result, the electrochemical performance of lithium-rich cathode materials was sensitive to the local composition in the bulk and at the surface of the as-prepared particles, which was highly associated with the synthesis process.

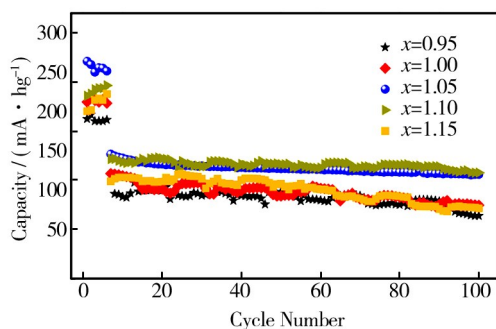


Fig. 7 Cyclic performance of the $\text{Li}_{1.2x}\text{Mn}_{0.54}\text{Ni}_{0.13}\text{Co}_{0.13}\text{O}_2$ electrodes when cycled between 2.0 and 4.8 V at room temperature (30 °C)

图 7 不同 Li 含量的 $\text{Li}_{1.2x}\text{Mn}_{0.54}\text{Ni}_{0.13}\text{Co}_{0.13}\text{O}_2$ 电极在 2.0 ~ 4.8 V, 30 °C 测试条件下的循环性能

4 Conclusions

In conclusion, this article reported herein provided new insights into the structural information and corresponding electrochemical properties of $\text{Li}_{1.2x}\text{Mn}_{0.54}\text{Ni}_{0.13}\text{Co}_{0.13}\text{O}_2$ ($x = 0.95, 1.00, 1.05, 1.10, \text{ and } 1.15$) materials as a function of x (Li content) utilized for the material synthesis via a co-precipitation method. With the increase in Li content, the excess of Li ions during the synthesis process could compensate for an evaporative lithium loss during the calcinations, resulting in the formation of spinel phase impurity in the local structure,

and even initiation of generating a small amount of Li_2CO_3 at the surface of the lithium-rich transition metal oxides as revealed by XRD, Raman, and XPS observations. The impurities in the bulk and at the surface originated from the varying amounts of Li ions would result in deviation of the as-prepared lithium-rich transition metal oxides from the ideal composition and microstructure of layered $\text{Li}_{1.2}\text{Mn}_{0.54}\text{Ni}_{0.13}\text{Co}_{0.13}\text{O}_2$, thereby impeding the electrochemical activation of the final lithiated oxide electrodes to some extent and provoking a change in the voltage-capacity profile. Our results further confirmed that the electrochemical performance of lithium-rich cathode materials was sensitive to the local structure in the bulk and at the surface, which was highly associated with the synthesis process of the materials. The as-prepared sample with 5% excess of Li in molar ratio utilized for the material synthesis showed better electrochemical performance in terms of discharge capacity (~ 270 mAh/g) and voltage profile in comparison to other as-prepared samples with different amounts of Li ions.

References

- [1] THACKERAY M M, WOLVERTON C, ISAACS E D. Electrical Energy Storage for Transportation—Approaching the Limits of, and Going beyond, Lithium-ion Batteries[J]. *Energy & Environmental Science*, 2012, 5: 7854—7863.
- [2] CHIKKANNANAVAR S B, BERNARDI D M, LIU L Y. A Review of Blended Cathode Materials for Use in Li-ion Batteries[J]. *Journal of Power Sources*, 2014, 248: 91—100.
- [3] HU M, PANG X L, ZHOU Z. Recent Progress in High-voltage Lithium Ion Batteries[J]. *Journal of Power Sources*, 2013, 237: 229—242.
- [4] HE P, YU H, LI D, et al. Layered Lithium Transition Metal Oxide Cathodes towards High Energy Lithium-ion Batteries[J]. *Journal of Materials Chemistry*, 2012, 5: 3680—3695.
- [5] THACKERAY M M, KANG S H, JOHNSON C S, et al. Li_2MnO_3 -Stabilized LiMO_2 ($M = \text{Mn, Ni, Co}$) Electrodes for Lithium-ion Batteries[J]. *Journal of Materials Chemistry*, 2007, 17: 3112—3125.
- [6] LU Z H, DAHN J R. Understanding the Anomalous Capacity of $\text{Li/Li}[\text{Ni}_x\text{Li}_{(1/3-2x/3)}\text{Mn}_{(2/3-x/3)}]\text{O}_2$ Cells Using in situ X-ray Diffraction and Electrochemical Studies[J]. *Journal of Electrochemical Society*, 2002, 149: A815—A822.
- [7] LU Z, MACNEIL D D, DAHN J R. Layered Cathode Materials $\text{Li/Li}[\text{Ni}_x\text{Li}_{(1/3-2x/3)}\text{Mn}_{(2/3-x/3)}]\text{O}_2$ for Lithium-ion Bat-

- teries [J]. *Electrochemical Solid-state Letters*, 2001, 4: A191—A194.
- [8] ARMSTRONG A R, HOLZAPFEL M, NOVAK P, et al. Demonstrating Oxygen Loss and Associated Structural Reorganization in the Lithium Battery Cathode $\text{Li}[\text{Ni}_{0.2}\text{Li}_{0.2}\text{Mn}_{0.6}]\text{O}_2$ [J]. *Journal of American Chemical Society*, 2006, 128: 8694—8698.
- [9] ITO A, LI D, SATO Y, et al. Cyclic Deterioration and Its Improvement for Li-rich Layered Cathode Material $\text{Li}[\text{Ni}_{0.17}\text{Li}_{0.2}\text{Co}_{0.07}\text{Mn}_{0.56}]\text{O}_2$ [J]. *Journal of Power Sources*, 2010, 195: 567—573.
- [10] SATHIYA M, ROUSSE G, RAMESHA K, et al. Reversible Anionic Redox Chemistry in High-capacity Layered-oxide Electrodes [J]. *Nature Materials*, 2013, 12: 827—835.
- [11] BOULINEAU A, SIMONIN L, COLIN J F, et al. Evolutions of $\text{Li}_{1.2}\text{Mn}_{0.61}\text{Ni}_{0.18}\text{Mg}_{0.01}\text{O}_2$ during the Initial Charge/Discharge Cycle Studied by Advanced Electron Microscopy [J]. *Chemistry of Materials*, 2012, 24: 3558—3566.
- [12] YABUUCHI N, YOSHII K, MYUNG S T, et al. Detailed Studies of a High-capacity Electrode Material for Rechargeable Batteries, Li_2MnO_3 - $\text{LiCo}_{1/3}\text{Ni}_{1/3}\text{Mn}_{1/3}\text{O}_2$ [J]. *Journal of American Chemical Society*, 2011, 133: 4404—4419.
- [13] BARENO J, LEI C H, WEN J G, et al. Local Structure of Layered Oxide Electrode Materials for Lithium-ion Batteries [J]. *Advanced Materials*, 2010, 22: 1122—1127.
- [14] LIU J L, WAN G J, XIA Y Y. A New Rechargeable Lithium-ion Battery with a $x\text{Li}_2\text{MnO}_3 \cdot (1-x)\text{LiMn}_{0.4}\text{Ni}_{0.4}\text{Co}_{0.2}\text{O}_2$ Cathode and a Hard Carbon Anode [J]. *Electrochimica Acta*, 2011, 56: 7392—7396.
- [15] OHZUKU T, NAGAYAMA M, TSUJI K, et al. High-capacity Lithium Insertion Materials of Lithium Nickel Manganese Oxides for Advanced Lithium-ion Batteries: toward Rechargeable Capacity More than 300 mAh/g [J]. *Journal of Materials Chemistry*, 2011, 21: 10179—10188.
- [16] LIU J L, CHEN L, HOU M, et al. General Synthesis of $x\text{Li}_2\text{MnO}_3 \cdot (1-x)\text{LiMn}_{1/3}\text{Ni}_{1/3}\text{Co}_{1/3}\text{O}_2$ Nanomaterials by a Molten-salt Method: towards a High Capacity and High Power Cathode for Rechargeable Lithium Batteries [J]. *Journal of Materials Chemistry*, 2012, 22: 25380—25387.
- [17] KANG S H, AMINE K. Synthesis and Electrochemical Properties of Layer-structured $0.5\text{Li}(\text{Ni}_{0.5}\text{Mn}_{0.5})\text{O}_2 \cdot 0.5\text{Li}(\text{Li}_{1/3}\text{Mn}_{2/3})\text{O}_2$ Solid Mixture [J]. *Journal of Power Sources*, 2003, 124: 533—537.
- [18] KIM M G, JO M, HONG Y S, et al. Template-free Synthesis of $\text{Li}[\text{Ni}_{0.25}\text{Li}_{0.15}\text{Mn}_{0.6}]\text{O}_2$ Nanowires for High Performance Lithium Battery Cathode [J]. *Chemical Communications*, 2009, 2: 218—220.
- [19] HONG J, SEO D H, KIM S W, et al. Structural Evolution of Layered $\text{Li}_{1.2}\text{Ni}_{0.2}\text{Mn}_{0.6}\text{O}_2$ upon Electrochemical Cycling in a Li Rechargeable Battery [J]. *Journal of Materials Chemistry*, 2010, 20: 10179—10186.
- [20] GU M, BELHAROUAK I, ZHEN G J, et al. Formation of the Spinel Phase in the Layered Composite Cathode Used in Lithium Batteries [J]. *ACS Nano*, 2013, 7: 760—767.
- [21] LIU J L, LIU J, WANG R, et al. Degradation and Structural Evolution of $x\text{Li}_2\text{MnO}_3 \cdot (1-x)\text{LiMn}_{1/3}\text{Ni}_{1/3}\text{Co}_{1/3}\text{O}_2$ during Cycling [J]. *Journal of Electrochemical Society*, 2014, 161: A160—A167.
- [22] WEI G Z, LU X, KE F S, et al. Crystal Habit-tuned Nanoplate Material of $\text{Li}[\text{Li}_{1/3-2x/3}\text{Ni}_x\text{Mn}_{2/3-x/3}]\text{O}_2$ for High-rate Performance Lithium-ion Batteries [J]. *Advanced Materials*, 2010, 22: 4364—4367.
- [22] BOMMEL A V, DAHN J R. Kinetics Study of the High Potential Range of Lithium-rich Transition-metal Oxides for Lithium-ion Batteries by Electrochemical Methods [J]. *Electrochemical Solid-state Letters*, 2010, 13: A62—A64.
- [24] KIM M G, JO M, HONG Y S, et al. Template-free Synthesis of $\text{Li}[\text{Ni}_{0.25}\text{Li}_{0.15}\text{Mn}_{0.6}]\text{O}_2$ Nanowires for High Performance Lithium Battery Cathode [J]. *Chemical Communications*, 2009, 2: 218—220.
- [25] HE W, QIAN J, CAO Y, et al. Improved Electrochemical Performances of Nanocrystalline $\text{Li}[\text{Li}_{0.2}\text{Mn}_{0.54}\text{Ni}_{0.13}\text{Co}_{0.13}]\text{O}_2$ Cathode Material for Li-ion Batteries [J]. *RSC Advances*, 2012, 2: 3423—3429.
- [26] CROY J R, KIM D, BALASUBRAMANIAN M, et al. Countering the Voltage Decay in High Capacity $x\text{Li}_2\text{MnO}_3 \cdot (1-x)\text{LiMO}_2$ Electrodes ($M = \text{Mn}, \text{Ni}, \text{Co}$) for Li^+ -ion Batteries and Energy Storage [J]. *Journal of Electrochemical Society*, 2012, 159: A781—A790.
- [27] LIU W, FANG G, XIA B, et al. Improved Electrochemical Properties of $\text{Li}[\text{Li}_{0.2}\text{Ni}_{0.17}\text{Mn}_{0.56}\text{Co}_{0.07}]\text{O}_2$ Cathode Material via Micro-Structural Rearrangement [J]. *RSC Advances*, 2013, 3: 15630—15635.
- [28] LIU J L, HOU M, YI J, et al. Improving the Electrochemical Performance of Layered Lithium-rich Transition-metal Oxides by Controlling the Structural Defects [J]. *Energy & Environmental Science*, 2014, 7: 705—714.
- [29] WU Y, MANTHIRAM A. Effect of Surface Modifications on the Layered Solid Solution Cathodes $(1-z)\text{Li}[\text{Li}_{1/3}\text{Mn}_{2/3}]\text{O}_2$ - $(z)\text{Li}[\text{Mn}_{0.5-y}\text{Ni}_{0.5-y}\text{Co}_{2y}]\text{O}_2$ [J]. *Solid-state Ionics*, 2009, 180: 50—56.
- [30] PARK M S, LEE J W, CHOI W, et al. On the Surface Modifications of High-voltage Oxide Cathodes for Lithium-ion Batteries: New Insight and Significant Safety Improvement [J]. *Journal of Materials Chemistry*, 2010, 20: 7208—7213.

- Metal-free Oxygen Reduction in Alkaline Medium on High-surface-area Mesoporous Nitrogen-doped Carbons Made from Ionic Liquids and Nucleobases[J]. *Journal of the American Chemical Society*, 2010, 133(2): 206—209.
- [34] LIANG J, ZHENG Y, CHEN J, et al. Facile Oxygen Reduction on a Three-dimensionally Ordered Macroporous Graphitic C_3N_4 /Carbon Composite Electrocatalyst [J]. *Angewandte Chemie International Edition*, 2012, 51(16): 3892—3896.
- [35] AI K, LIU Y, RUAN C, et al. sp² C-dominant N-doped Carbon Sub-micrometer Spheres with a Tunable Size: A Versatile Platform for Highly Efficient Oxygen-reduction Catalysts [J]. *Advanced Material*, 2013, 25: 998—1003.
- [36] YOU C, LIAO S, LI H, et al. Uniform Nitrogen and Sulfur Co-doped Carbon Nanospheres as Catalysts for the Oxygen Reduction Reaction[J]. *Carbon*, 2014, 69: 294—301.
- [37] LEFEVRE M, PROIETTI E, JAOUEN F, et al. Iron-based Catalysts with Improved Oxygen Reduction Activity in Polymer Electrolyte Fuel Cells[J]. *Science*, 2009, 324(5923): 71—74.
- [38] PROIETTI E, JAOUEN F, LEFÈVRE M, et al. Iron-based Cathode Catalyst with Enhanced Power Density in Polymer Electrolyte Membrane Fuel Cells [J]. *Nature Communications*, 2011, 2: 416—424.
- [39] WU G, ARTYUSHKOVA K, FERRANDON M, et al. Performance Durability of Polyaniline-derived Non-precious Cathode Catalysts [J]. *ECS Transactions*, 2009, 25(1): 1299—1311.
- [40] WU G, MORE K, JOHNSTON C, et al. High-performance Electrocatalysts for Oxygen Reduction Derived from Polyaniline, Iron, and Cobalt [J]. *Science*, 2011, 332(6028): 443—447.
-
- (上接第 23 页)
- [31] WU F, LI N, SU Y, et al. Can Surface Modification Be More Effective to Enhance the Electrochemical Performance of Lithium Rich Materials? [J]. *Journal of Materials Chemistry*, 2012, 22: 1489—1497.
- [32] CROY J R, BALAUBRAMANIAN M, KIM D, et al. Designing High-capacity, Lithium-ion Cathodes Using X-ray Absorption Spectroscopy [J]. *Chemistry of Materials*, 2011, 23: 5415—5424.
- [33] LIU Y J, LIU S B, WANG Y P, et al. Effect of MnO_2 Modification on Electrochemical Performance of $LiNi_{0.2}Li_{0.2}Mn_{0.6}O_2$ Layered Solid Solution Cathode [J]. *Journal of Power Sources*, 2013, 222: 455—460.
- [34] SUN Y K, LEE M J, YOON C H, et al. The Role of AlF₃ Coatings in Improving Electrochemical Cycling of Li-Enriched Nickel-Manganese Oxide Electrodes for Li-ion Batteries [J]. *Advanced Materials*, 2012, 24: 1192—1196.
- [35] SONG B, LIU H, LIU Z, et al. High Rate Capability Caused by Surface Cubic Spinels in Li-rich Layer-structured Cathodes for Li-ion Batteries [J]. *Scientific Reports*, 2013, 3: 3094.
- [36] ABOUIMRANE A, COMPTON O C, DENG H, et al. Improved Rate Capability in a High-capacity Layered Cathode Material via Thermal Reduction Batteries and Energy Storage [J]. *Electrochemical and Solid-state Letters*, 2011, 14: A126—A129.
- [37] CHEN Z, QIN Y, AMINE K, et al. Role of Surface Coating on Cathode Materials for Lithium-ion Batteries [J]. *Journal of Materials Chemistry*, 2010, 20: 7606—7612.
- [38] BADDOUR-HADIEAN R, PEREIRA-RAMOS J. Raman Microspectrometry Applied to the Study of Electrode Materials for Lithium Batteries [J]. *Chemical Reviews*, 2010, 110: 1278—1319.